

Assessment of sulfur and iron speciation in a soil aggregate by combined S and Fe micro-XANES: microspatial patterns and relationships

Jörg Prietzel,^{a*} Jürgen Thieme^b and Murielle Salomé^c

^aLehrstuhl für Bodenkunde, Technische Universität München, Emil-Ramann-Strasse 2, D-85354 Freising, Germany, ^bInstitut für Röntgenphysik, Georg-August-Universität Göttingen, Friedrich-Hund-Platz 1, D-37077 Göttingen, Germany, and ^cX-ray Microscopy Beamline ID 21, European Synchrotron Radiation Facility, POB 220, 38043 Grenoble Cedex, France.
E-mail: prietzel@wzw.tum.de

To test whether synchrotron-based spectromicroscopy can be used to identify spatial patterns of sulfur (S) and iron (Fe) speciation as well as relationships between the speciation of S and Fe in soil colloids or aggregates at the micrometre and sub-micrometre level, an anoxically prepared dissected soil aggregate (size $\sim 1 \text{ mm}^3$) was analyzed by μ -XANES at the *K*-edges of S (2472 eV) and Fe (7112 eV). The experiment included (i) elemental mapping at the S *K*-edge (S, Si, Al) and the Fe *K*-edge (Fe, Si), (ii) acquisition of $300 \mu\text{m} \times 300 \mu\text{m}$ images of the region of interest with X-ray energies of 2474 eV (addressing reduced organic and inorganic S), 2483 eV (total S), 7121 eV (divalent Fe) and 7200 eV (total Fe), as well as (iii) acquisition of S and Fe μ -XANES spectra at two different positions, where image analysis suggested the dominance of reduced and oxidized S and Fe, respectively. Image analysis revealed a heterogeneous distribution of total Si, S and Fe as well as of different S and Fe species in the aggregate. Microregions which were either enriched in reduced or in oxidized S and Fe could be identified. A microregion with a large contribution of oxidized S (sulfate, sulfonate) to total S contained exclusively Fe(III) oxyhydroxides (probably ferrihydrite) as S-bearing phase, whereas another microregion with a large contribution of reduced organic S (thiol, organic disulfide) to total S contained a small amount of Fe(II)-bearing silicate in addition to the dominating Fe(III) oxyhydroxides. Our results show that combined S and Fe μ -XANES is a powerful tool for studying microscale spatial patterns of S and Fe speciation as well as microscale relationships between the speciation of S and Fe in soil aggregates.

1. Introduction

The cycling of sulfur (S) and iron (Fe) in soils and sediments is tightly coupled (Giblin & Howarth, 1984; Kostka & Luther III, 1995; Paul *et al.*, 2006). Both elements are highly susceptible to changes of the redox potential (Fe^{2+} versus Fe^{3+} ; S^{2-} versus SO_4^{2-}), and they readily react with each other in various ways (sorption, precipitation, redox reactions). This is particularly true for free (*e.g.* aqueous) and amorphous S and Fe species, and to a considerable extent also for crystallized Fe sulfides and oxyhydroxides, whereas reactions of S with silicate-bonded Fe are negligible. In well aerated soils and oxic sediments, the oxidized species of both elements coexist; under acidic conditions, Fe(III) oxyhydroxides are strong adsorbents

for SO_4^{2-} (Chao *et al.*, 1964; Turner & Kramer, 1992). Additionally, for particular soils and sediments the presence of Fe hydroxy sulfate precipitates has been reported (Bigham *et al.*, 1990). Under anoxic and mesoxic conditions, inorganic sulfide and Fe^{2+} precipitate already at low concentration as FeS and FeS_2 owing to the small solubility product of Fe sulfide minerals (Starkey, 1965; Paul *et al.*, 2006). Recently, a close correlation between the oxidation states of S and Fe in different soil horizons and for a soil toposequence with different groundwater influence has been revealed by Prietzel *et al.* (2009), using synchrotron-based S and Fe *K*-edge XANES. In this paper we tested spatially resolving S and Fe *K*-edge μ -XANES that had been conducted on a dissected aggregate from the subsoil of a clayey soil derived from shale

for its ability to reveal microscale spatial patterns of S and Fe speciation as well as microscale relationships between the speciation of S and Fe in soil aggregates.

2. Materials and methods

We sampled the BC horizon of a clayey cambisol located near Balingen (SW Germany) that had formed by weathering of Jurassic shale (Lias ϵ ; Posidonienschiefer). The soil is deeply (>80 cm) weathered, characterized by a large clay content over the entire profile, and by large stocks of lithogenic organic C, N, P and S. Moreover, it is characterized by large contents of pedogenic Fe(III) oxyhydroxides (ferrihydrite, goethite). It is stocked with 100-yr-old Norway spruce (*Picea abies* L.) forest. Traditional methods of S speciation (Fischer, 1989) suggest the coexistence of sulfate, organic S and inorganic sulfide in the studied BC horizon.

The investigated horizon was rich in S (1.05 g kg^{-1}) and Fe; the large clay content together with frequent soil moisture changes resulted in formation of sharp-edged aggregates with diameters ranging from 2 to 5 mm. Several aggregates were sampled from that horizon under exclusion of oxygen by flushing with Ar. The aggregates were transported in field-moist state under Ar atmosphere and dried in the laboratory under N_2 atmosphere, thus preventing artificial changes of the oxidation states of S and Fe during sample transport, storage and drying. In the laboratory, a suitable aggregate (size $\sim 1 \text{ mm}^3$) was carefully dissected with a lancet. The dissected aggregate was attached to a Si_3N_4 window that had been mounted on a sample holder, using a Canada balsam/xylene mixture as described by Prietzel *et al.* (2007), with the dissected surface facing upward. The work was carried out in a glove box in a pure N_2 atmosphere; the sample was stored in an air-tight bottle under N_2 until analysis. As assured by visual inspection, the spatial distribution of the elements was not changed by the preparation (dissection): coloured micro-patterns (e.g. nodules, mottles) were not in any way distorted or spread out in the cut direction, but remained in their original structure.

S and Fe μ -XANES analyses were conducted using the scanning X-ray microscope (SXM) at beamline ID-21 of the European Synchrotron Radiation Facility (ESRF) in Grenoble, France (Barrett *et al.*, 2000). The instrument set-up, the parameters used for acquisition of the XANES images and spectra, and the techniques used for evaluation of the spectra have been described in detail by Prietzel *et al.* (2003, 2007). The SXM uses a Fresnel zone plate as focusing optics, which de-magnifies the synchrotron X-ray source, produced by an electron beam (energy: 6 GeV; average current: 180 mA), to generate a sub-micrometre probe with high flux. The monochromaticity of the beam and the energy scan were ensured by a fixed-exit double-crystal Si (111) monochromator located upstream of the microscope, which offers an energy resolution of 0.5 eV for both edges. The S X-ray transmission and fluorescence signals were recorded simultaneously with a Si photodiode mounted downstream of the sample and an energy-dispersive 30 mm^2 high-purity Ge detector (Princeton

Gamma-Tech), respectively. For each spectrum, the signals of ten scans were compiled. The energy calibration for S was carried out using pure CaSO_4 (white-line peak maximum: 2482.5 eV) and for Fe with Fe foil (edge step at 7112.0 eV).

Sulfur and iron analyses were conducted in June 2006 during two different beam time allocations. A square-shaped ($300 \mu\text{m} \times 300 \mu\text{m}$) region of interest which comprised the aggregate edge with a macropore, as well as the adjacent aggregate matrix (Fig. 1), was selected using a visible-light microscope (VLM), which is permanently mounted in the SXM. Then we performed elemental mapping (acquisition of X-ray fluorescence images of total Si and total S for the selected region of interest with an X-ray energy of 2483 eV). This energy is slightly larger than the *K*-edge of the most oxidized S species (sulfate, 2482.5 eV), and produces X-ray fluorescence signals from all possible S species that are present in soil (Prietzel *et al.*, 2003). Subsequently we acquired another X-ray fluorescence image with an X-ray energy of 2474 eV. With this energy, only the *K*-shell electrons of reduced organic and inorganic S, but not those of intermediate and highly oxidized S, are excited, and the fluorescence signal is exclusively produced by reduced organic and inorganic S species, such as inorganic sulfide, thiol and organic (di)sulfide. Finally, we selected two S-rich microregions (positions 1 and 2 indicated by arrows in Fig. 3). According to the X-ray fluorescence images, the sulfur at position 1 is primarily reduced S, whereas that at position 2 is mainly oxidized S. At both positions we acquired S *K*-edge μ -XANES spectra. According to the beam size at 2483 eV, the irradiated area was $0.3 \mu\text{m} \times 0.8 \mu\text{m}$. In the second beam time, we repeated the entire procedure at the Fe *K*-edge. At an energy of 7200 eV, which is sufficient to excite the *K*-shell electrons of all iron species irrespective of their oxidation state (Fe^0 , Fe^{2+} , Fe^{3+}), elemental mapping (Fe, Si) was performed for the same region of interest that had been investigated for S species before. The Si map was used to

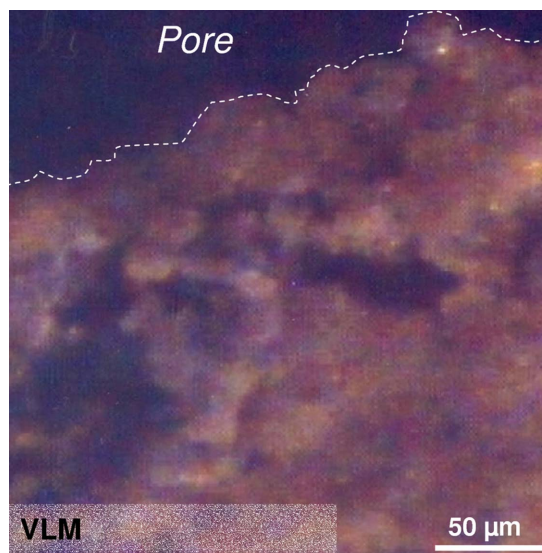


Figure 1
VLM image of a $300 \mu\text{m} \times 300 \mu\text{m}$ region of a dissected soil aggregate sampled from the BC horizon of a forest soil near Balingen, Germany.

match the images taken at the S and Fe *K*-edges. Subsequently, we acquired another X-ray fluorescence image with an X-ray energy of 7121 eV. At this energy, only *K*-shell electrons of elemental or divalent Fe, but not those of trivalent Fe, are excited, resulting in a fluorescence map specific for divalent Fe (elemental Fe is not present in soils). Finally, we acquired Fe *K*-edge μ -XANES spectra at positions 1 and 2, where S μ -XANES spectra had been recorded earlier. According to the beam size at 7200 eV, the irradiated area was $0.4 \mu\text{m} \times 1.2 \mu\text{m}$.

Sulfur and Fe *K*-edge XANES spectra were acquired in the energy range between 2450 and 2510 eV as well as between 7085 and 7255 eV for S and Fe, respectively. The dwell time was always 1 s, and the energy resolution was 0.5 eV. The spectra were acquired in fluorescence mode because the sample was too thick to permit transmission of X-rays.

The spectra were background-corrected and edge-normalized using the software *Athena* (Ravel & Newville, 2005). The energy ranges used for background correction were 2450–2461 eV for S and 7085–7100 eV for Fe; those used for normalization of the spectra were 2487–2510 eV (S) and 7210–7240 eV (Fe). Deconvolution of the S and Fe *K*-edge XANES spectra acquired at each of the two investigated positions and calculation of the contribution of different S and Fe species to total S and Fe, respectively, was carried out by linear combination fitting (LCF), using the LCF routine included in *Athena*. The predictor variables used for the LCF exercises conducted on the S *K*-edge XANES spectra were Fe monosulfide, pyrite, elemental S, cysteine (representing thiol and organic disulfide S), methionine sulfoxide, dimethyl sulfone, Na hexane sulfonate and Na sulfate (Fig. 2a). The predictor

variables used for deconvolution of the Fe *K*-edge XANES spectra included Fe monosulfide, pyrite, biotite (representing Fe in silicate), goethite and ferrihydrite (Fig. 2b). All standards had been diluted and finely ground with quartz to a concentration of $2000 \text{ mg S/Fe kg}^{-1}$ in order to minimize confounding self-absorption effects. Hematite was not included as predictor variable for Fe speciation because it is not present in the studied soil.

3. Results

The VLM image of the investigated part of the soil aggregate (Fig. 1) indicates a significant heterogeneity of aggregate structure and composition. The aggregate is apparently characterized by an intricate microstructure, comprising micro- and mesopores (dark), iron-oxide-rich (brown, reddish) and iron-oxide-poor (grey) regions. The silicon (Si) map (Figs. 3a and 3d) shows a heterogeneous distribution of Si: it is enriched in distinct zones, whereas large parts of the aggregate show markedly smaller Si concentrations. The spatial distribution of S (Fig. 3b) in the aggregate is also heterogeneous. There is no spatial correlation between S and Si, *i.e.* S-rich zones are neither particularly rich nor particularly poor in Si. In contrast to Si, the aggregate contains microregions ('hot spots') which are particularly enriched in S (red spots indicated by 'P' or '2' in Fig. 3b). Fig. 3(c) shows that reduced S, comprising S species with an oxidation state lower than +1, is also heterogeneously distributed in the aggregate. Comparison of Figs. 3(b) and 3(c) reveals (i) the existence of S-rich microregions (*e.g.* position 1) where reduced S seems to dominate strongly over oxidized S,

but also (ii) the presence of S hot spots (*e.g.* position 2) which contain almost no reduced S, suggesting a strong dominance of oxidized over reduced S. Also, the spatial distribution of Fe in the aggregate (Fig. 3e) is heterogeneous; Fe is concentrated in hot spots, which are mainly located in two Fe-rich regions of the aggregate. Comparison of Figs. 3(d) and 3(e) reveals that regions with particularly large Si concentrations seem to contain less Fe than regions with small Si concentrations. No spatial correlation between the concentration of total S and total Fe in the aggregate is evident (Figs. 3b and 3e). Most regions with elevated Fe concentrations are enriched in divalent Fe (Figs. 3e and 3f); there are only a few areas which contain a significant amount of total Fe but only little divalent Fe. Comparison of positions 1 and 2 in Figs. 3(e) and 3(f) suggests that the contribution of reduced Fe to total Fe is larger at position 1 than at position 2. As shown above, sulfur maps acquired at different energies had also indicated a markedly

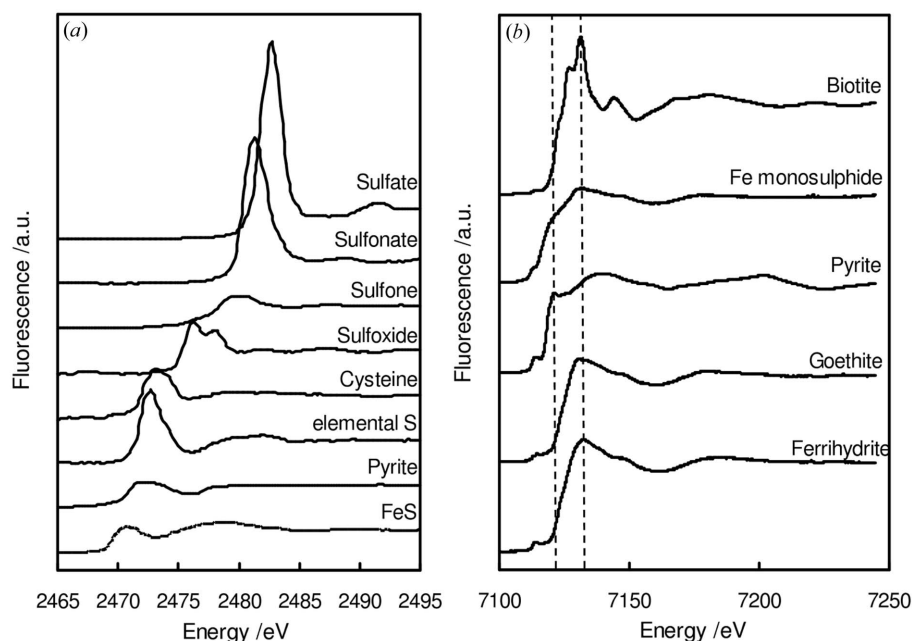


Figure 2

(a) S *K*-edge spectra of the reference compounds Fe monosulfide, pyrite, elemental S, L-cysteine, methionine sulfoxide, dimethyl sulfone, Na hexane sulfonate and Na sulfate. (b) Fe *K*-edge spectra of the reference compounds ferrihydrite, goethite, pyrite, Fe monosulfide and biotite used for the LCF analyses. All standards were diluted and finely ground with quartz to a concentration of $2000 \text{ mg S and Fe kg}^{-1}$.

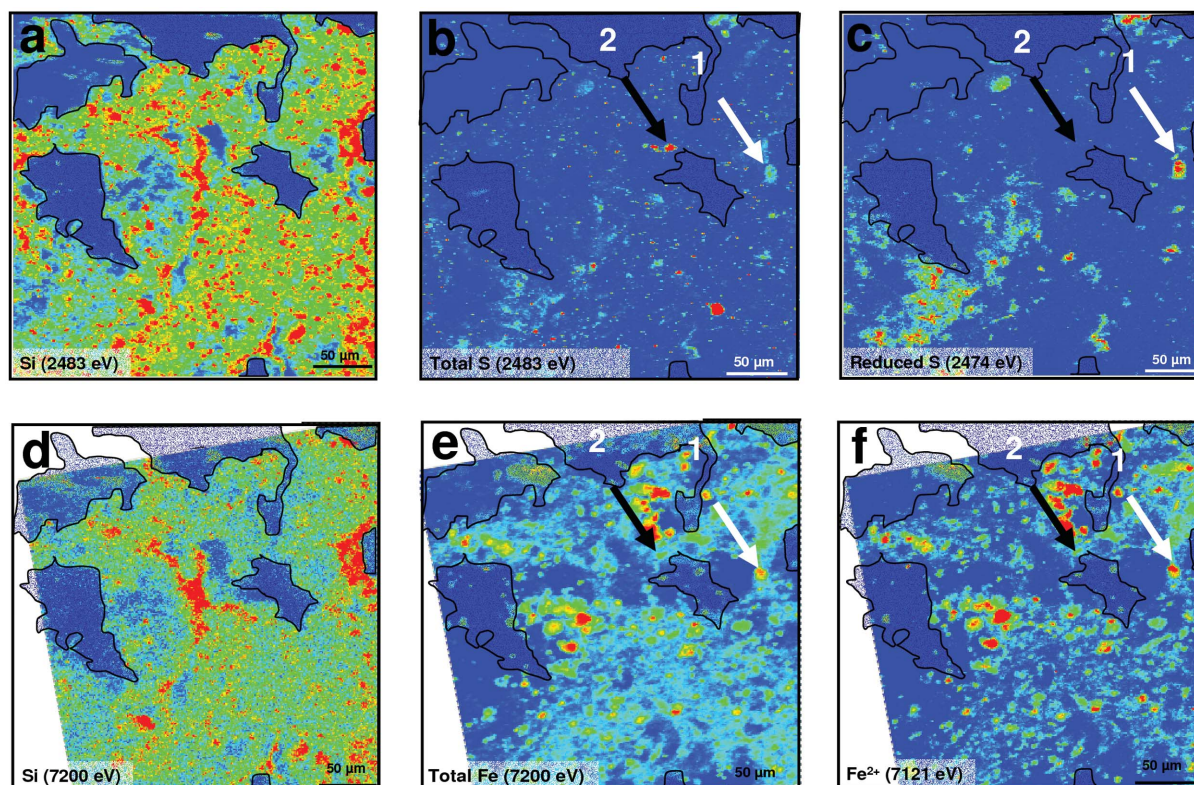


Figure 3

X-ray fluorescence maps of a $300\ \mu\text{m} \times 300\ \mu\text{m}$ region of interest in a dissected soil aggregate sampled from the BC horizon of a forest soil near Balingen, Germany. (a) Map of total Si acquired with an X-ray energy of 2483 eV. (b) Map of total S acquired with an X-ray energy of 2483 eV. (c) Map of reduced S acquired with an X-ray energy of 2474 eV. (d) Map of total Si acquired with an X-ray energy of 7200 eV. (e) Map of total Fe acquired with an X-ray energy of 7200 eV. (f) Map of elemental and divalent Fe acquired with an X-ray energy of 7121 eV. In maps (b)–(f), increasing concentrations of the elements or element species of interest are represented by a colour change in the sequence blue–green–yellow–red.

larger contribution of reduced S to total S at position 1 than at position 2. Thus, a comprehensive evaluation of the S and Fe maps acquired at energies representing reduced and total S and Fe, respectively, suggests a spatial correlation of the S and Fe oxidation state in the investigated soil aggregate on the micrometre scale.

The S *K*-edge μ -XANES spectra taken at positions 1 and 2 (Figs. 4a and 4c) support the conclusions based on the image evaluation. The normalized S *K*-edge XANES spectrum of position 1 (Fig. 4a) is characterized by a large peak at an energy of 2474 eV, representing reduced organic S species such as thiol or organic disulfide; the additional peak at 2480 eV indicates the presence of sulfone. No peaks with white lines at 2469 or 2482.5 eV can be identified, hence inorganic sulfide or sulfate do not appear to be present at position 1. Contrastingly, the spectrum acquired at position 2 is strongly dominated by one large peak with a white line at 2482.5 eV which represents sulfate. Deconvolution of the spectrum by LCF (Table 1) showed that the sulfur at position 1 is mainly organic disulfide or thiol (63% of total S), accompanied by organic S species of intermediate oxidation states (sulfoxide, sulfone, sulfonate). No inorganic sulfide or sulfate is present. At position 2, sulfate contributes 40% of total S; LCF additionally revealed a contribution of 53% sulfone and of 7% sulfonate to the total S pool of position 2. In contrast to

position 1, no reduced organic S species were identified by LCF. In summary, the sulfur on average is more oxidized and more inorganic at position 2 compared with position 1. The normalized Fe *K*-edge spectra at positions 1 and 2 differ only slightly from each other (Figs. 3b and 3d). Both spectra look very much like the reference spectra of goethite or ferrihydrite (Fig. 2b). However, the Fe *K*-edge XANES white line at position 1 has a slightly smaller energy (7131 eV) than that at position 2 (7133 eV), suggesting the presence of an Fe(II)-bearing phase in addition to the dominating Fe(III) phase. Calculation of the contribution of different Fe species by LCF (Table 2) shows that the Fe at both positions is exclusively (position 2) or almost exclusively (97%; position 1) Fe(III) oxyhydroxide. According to the LCF results, 3% of the Fe at position 1 are silicate-bound (reference compound biotite), whereas no silicate-bound Fe is present at position 2. Iron sulfide minerals were not identified at either position.

4. Discussion

Our study shows that combined S and Fe μ -XANES is a suitable tool for studying microscale spatial patterns of the S and Fe speciation as well as microscale relationships between the speciation of S and Fe in soil aggregates. It could be shown that the total S and Fe, but also S and Fe species of different

Table 1

Contribution of different S species to total sulfur at positions 1 and 2 in the studied soil aggregate as calculated by linear combination fitting on the S *K*-edge XANES spectra shown in Fig. 4(a) and the spectra of the predictor compounds shown in Fig. 2(a).

	FeS S (%)	Pyrite S (%)	Elemental S (%)	Thiol/organic disulfide S (%)	Sulfoxide S (%)	Sulfone S (%)	Sulfonate S (%)	Sulfate S (%)	<i>R</i> value	Reduced χ^2
S oxidation state	-2	-1	0	+0.2 to +0.5	+2	+4	+5	+6		
Position 1	0	0	0	61	16	16	7	0	0.00520	0.657
Position 2	0	0	0	0	0	53	7	40	0.01095	6.132

Table 2

Contribution of different Fe species to total iron at positions 1 and 2 in the studied soil aggregate as calculated by linear combination fitting on the Fe *K*-edge XANES spectra shown in Fig. 4(b) and the spectra of the predictor compounds shown in Fig. 2(b).

	FeS Fe (%)	Pyrite Fe (%)	Biotite Fe (%)	Ferrihydrite Fe (%)	Goethite Fe (%)	<i>R</i> value	Reduced χ^2
Fe oxidation state	+2	+2	+2.3	+3	+3		
Position 1	0	0	3	97	0	0.00276	1.667
Position 2	0	0	0	100	0	0.00342	1.920

oxidation states, are distributed heterogeneously in the investigated aggregate. In contrast to earlier studies conducted on various soils with different redox status at the landscape scale (Prietz et al., 2009), in our study no spatial colocalization of reduced S and Fe species could be proven for the two microregions of the aggregate that had been investigated in more detail by combined μ -S and μ -Fe XANES. At position 2, the local absence of reduced S and enrichment of sulfate are associated with an absence of reduced Fe and enrichment of

oxidized Fe (ferrihydrite). This colocalization can easily be explained by precipitation of sulfate with Fe³⁺ as Fe hydroxy sulfate (Bigham et al., 1990) or adsorption of sulfate to pedogenic Fe(III) minerals such as ferrihydrite or goethite (Chao et al., 1964; Turner & Kramer, 1992). In contrast, at position 1 oxidized Fe (ferrihydrite) is associated with reduced S. At first glance, such a colocalization does not comply with thermodynamic constraints (reduced inorganic S cannot

coexist with oxidized Fe). However, the reduced sulfur accumulated at position 1 is not inorganic (e.g. pyrite or Fe monosulfide) but organic S (thiol and organic disulfide). In contrast to inorganic sulfide, reduced organic S bound in soil organic matter can co-exist with Fe oxyhydroxides, e.g. as organic disulfide-containing humic compounds adsorbed to or interspersed with pedogenic Fe minerals. Unfortunately, only one position with enrichment of reduced S has been investigated in our study; at other positions, where inorganic sulfide

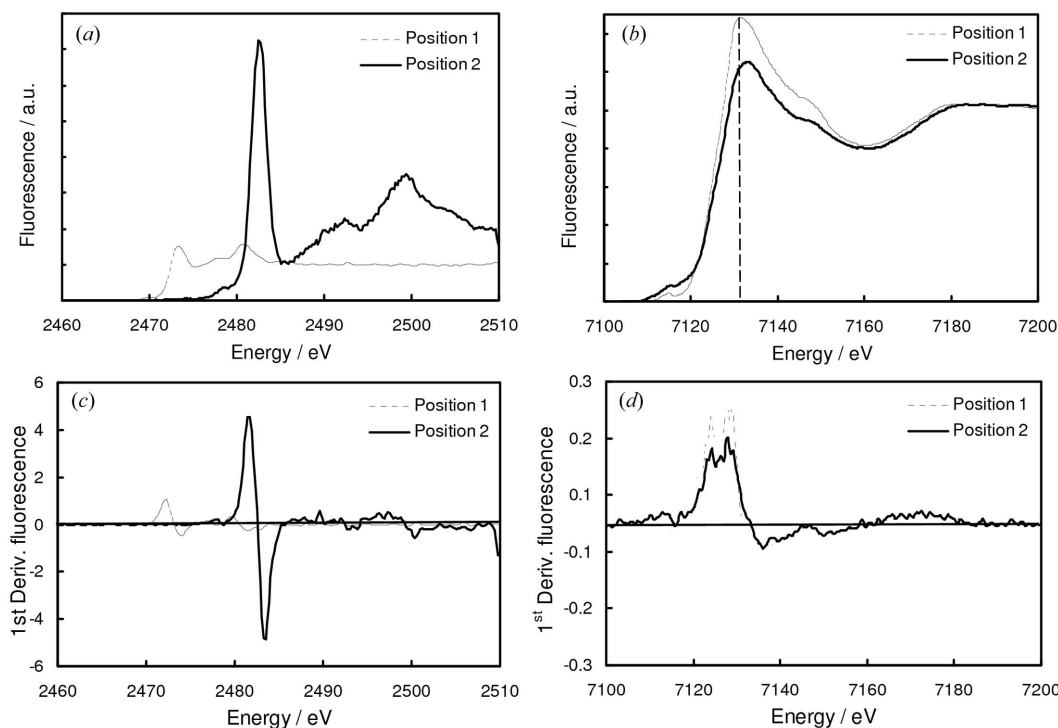


Figure 4

Baseline-corrected edge-normalized sulfur (a) and iron (b) *K*-edge XANES spectra and their first derivatives (c, d) acquired at positions 1 and 2 of the dissected soil aggregate sampled from the BC horizon of a forest soil near Balingen, Germany.

may contribute significantly to reduced S, an enrichment of divalent Fe should be expected.

It must be pointed out that the comparison of S and Fe X-ray fluorescence microprobe maps acquired at two different energies for each element did not yield an exact ratio between reduced and oxidized S or Fe species for each pixel. Mapping rather identified microregions which were relatively enriched or depleted in reduced or oxidized S/Fe. These regions were subsequently investigated in more detail by acquisition of *K*-edge μ -XANES spectra. The lack of an exact species ratio in the maps is due to 'cross-talk' effects among different species with different oxidation states and/or different shapes of their XANES spectra. Thus, for example, irradiation of a certain microregion with X-rays of energy 2483 eV resulted in a signal which was not exclusively produced by the white line and scatter of sulfate, but additionally included components produced by scatter and white-line tails of less oxidized S species (e.g. sulfonates, sulfones) which may also have been present at that particular microregion. The same is true when the sample is irradiated with X-rays of energy 2474 eV. Here, the fluorescence signal is not exclusively produced by reduced organic S such as thiol and organic disulfide; it additionally may contain components produced by scatter and white-line tails of elemental S and/or inorganic sulfides. Deconvolution of these combined non-linear effects is complicated (Pickering *et al.*, 2000) and requires sophisticated computerized algorithms even for systems with fewer probable species as was the case for S in our study.

Our results must be interpreted with some caution, because they might have been affected by several confounding factors and interferences (Lombi & Susini, 2009; Kelly *et al.*, 2008), namely (i) self absorption, (ii) photo-oxidation/photo-reduction and (iii) problems involved with the different spatial resolution and penetration depth of X-rays at the S and Fe *K*-edge energies, respectively. Self-absorption leads to an attenuation of X-ray fluorescence peaks, which may cause problems in the correct identification of element species in LCF exercises conducted on fluorescence spectra; furthermore, it may result in an incorrect quantification of the affected elements and element species. Self-absorption is particularly strong for highly concentrated coarse-grained particles of the element of interest (Kelly *et al.*, 2008). In principle, it can be reduced or even eliminated by appropriate dilution and/or grinding of the sample; however, this is impossible when undisturbed soil aggregates are investigated. In our study, the size of the S and Fe hot spots seems to be less than 10 μm , which is in the range of (S) or considerably smaller than (Fe) the penetration depths of X-rays in quartz-dominated mineral soils at the S and Fe *K*-edges (absorption length of quartz at 2480 and 7200 eV: 4 and 77 μm , respectively; Elam *et al.*, 2002; Ravel & Newville, 2005). Moreover, for Fe, transmission spectra were also available, which after background correction and normalization looked identical to the fluorescence spectra. Furthermore, our reference compounds had been diluted and finely ground with quartz to an S and Fe concentration of 2000 mg kg⁻¹ prior to acquisition

of XANES spectra. Thus we assume that self-absorption in our study was not a serious problem.

Artificial changes of the sample owing to photo-reduction and/or photo-oxidation are a particular danger with μ -XANES, where the X-ray beam is focused on a small sample area, resulting in a large energy flux density. We addressed this problem by collecting several spectra, each of which taken with a short irradiation time. Photo-reduction and/or photo-oxidation effects thus can be identified and quantified by comparing the first with the last spectra. For the S μ -XANES measurements, the spectra were identical; significant photo-reduction and/or photo-oxidation of S compounds thus could be ruled out. The same was done during the second beam time for the Fe μ -XANES measurements; again the spectra of the first and the last measurement looked identical. Thus also for Fe, artificial speciation changes owing to photo-reduction or photo-oxidation seem unlikely. Unnoticed changes of Fe speciation might have occurred during acquisition of the S XANES spectra in the first beam time; however, such changes are unlikely, because the X-ray energy at the S *K*-edge (2470 eV) is only 30% of the Fe *K*-edge energy (7200 eV), and irradiation with X-rays at the Fe *K*-edge has not resulted in significant photo-oxidation or reduction of Fe species.

In our study, images of the sample surface were acquired with a pixel size of 1 $\mu\text{m} \times 1 \mu\text{m}$ for S and Fe. However, it must be considered that the true lateral resolution in the *x-y* plane (surface of the sample) is also determined by the beam size, which was 0.3 $\mu\text{m} \times 0.8 \mu\text{m}$ for S and 0.4 $\mu\text{m} \times 1.2 \mu\text{m}$ for Fe. Moreover, the spatial resolution is much larger than the lateral resolution, because it is also determined by the length of the irradiated zone in the *z*-direction (way through the aggregate, orthogonal to the *x-y* plane) (Lombi & Susini, 2009). The latter is determined either by the thickness of the sample (thin samples for which X-ray transmission images at all X-ray energies of interest are possible) or by the penetration depth of the irradiated X-rays at these energies (thicker samples). In our case, where a dissected aggregate was investigated and transmission images could only be acquired at the Fe *K*-edge energy, the overall fluorescence signal includes and summarizes weighted fluorescence signals from different depths (*z*-direction) of the aggregate, ranging from the surface to a depth of $\sim 4 \mu\text{m}$ (absorption length of SiO₂, the principal constituent of most mineral soils, at 2483 eV) and 77 μm (absorption depth of SiO₂ at 7200 eV; Elam *et al.*, 2002; Ravel & Newville, 2005) for Fe. Generally, the relative contribution of the different signals originating from the excitation of S and Fe core electrons from atoms located at different aggregate 'depths' (*z*-direction positions) decreases exponentially from the surface of the dissected aggregate to its interior, but much more pronounced for S than for Fe. This implies that the minimum 'true' spatial resolution for fluorescence images and μ -XANES analyses of Fe and S in samples is (i) different and (ii) (in most cases considerably) larger than the lateral resolution, unless the thickness of the sample is less than 1 μm . Consequently, for any sample of heterogeneous composition which is thicker than 1 μm , a perfect true spatial correlation of

reduced S with divalent Fe and of oxidized S with trivalent Fe species would also result in an imperfect apparent correlation owing to the different irradiation depth profiles for both elements.

The general problem of self-absorption as well as the confounding effect of different penetration depths of X-rays during μ -XANES studies of S and Fe speciation in soils in principle may be overcome by appropriate techniques (i) to produce ultra-thin ($<5\ \mu\text{m}$) sections of soil aggregates under anoxic conditions, and (ii) to protect these thin sections against oxygenation during the period between sample preparation and analysis. Finally, the difference between spatial *versus* lateral resolution (Lombi & Susini, 2009) would be decreased; however, even for a thin section with a thickness of $2\ \mu\text{m}$, the spatial resolution in the x - y plane (sample surface) which is determined by the size of the X-ray beam (in our study $0.3\ \mu\text{m} \times 0.8\ \mu\text{m}$ for S and $0.4\ \mu\text{m} \times 1.2\ \mu\text{m}$ for Fe) would still be 2.5 to 7 times (S) and 2 to 5 times (Fe) smaller compared with the irradiated zone in the z -direction (way through the aggregate, orthogonal to the x - y plane). Recently, we were successful in producing a thin section of a soil aggregate embedded in S-free resin under anoxic conditions with a thickness of about $10\ \mu\text{m}$; it can be expected that anoxically prepared thin sections with a thickness of $<2\ \mu\text{m}$ will be available for the investigation of soil aggregates in the near future. Such thin sections will allow an even more detailed and accurate element speciation on the micrometre and sub-micrometre scale. Additionally, the ongoing development of more efficient and sensitive detectors will allow the acquisition of XANES spectra and images with strongly decreased X-ray photon fluxes, which will help to reduce confounding photo-reduction and photo-oxidation artifacts (Lombi & Susini, 2009).

We gratefully acknowledge the support of this study by grants of the European Synchrotron Radiation Facility (ESRF; proposals ME-1267 and EC-30).

References

- Barrett, R., Kaulich, B., Salomé, M. & Susini, J. (2000). *6th International Conference on X-ray Microscopy*, 2–6 August 1999, Berkeley, CA, USA, edited by W. Meyer-Ilse, T. Warwick and D. Attwood, p. 458. Melville: American Institute of Physics.
- Bigham, J. M., Schwertmann, U., Carlson, L. & Murad, E. (1990). *Geochim. Cosmochim. Acta*, **54**, 2743–2758.
- Chao, T. T., Harvard, M. E. & Fang, S. (1964). *Soil Sci. Soc. Am. Proc.* **18**, 632–635.
- Elam, W. T., Ravel, B. & Sieber, J. R. (2002). *Radiat. Phys. Chem.* **63**, 21–128.
- Fischer, M. (1989). *Forstl. Forschungsber. München*, **100**, 1–245.
- Giblin, A. E. & Howarth, R. W. (1984). *Limnol. Oceanogr.* **29**, 47–63.
- Kelly, S. D., Hesterberg, D. & Ravel, B. (2008). *Methods of Soil Analysis*, Part 5. *Mineralogical Methods*, pp. 387–464. Madison: Soil Science Society of America.
- Kostka, J. E. & Luther III, G. W. (1995). *Biogeochemistry*, **29**, 159–181.
- Lombi, E. & Susini, J. (2009). *Plant Soil*, **320**, 1–35.
- Paul, S., Küsel, K. & Alewell, C. (2006). *Soil Biol. Biochem.* **38**, 1028–1039.
- Pickering, I. J., Prince, R. C., Salt, D. E. & George, G. N. (2000). *Proc. Natl. Acad. Sci. USA*, **97**, 10717–10722.
- Prietzl, J., Thieme, J., Eusterhues, K. & Eichert, D. (2007). *Eur. J. Soil Sci.* **58**, 1027–1041.
- Prietzl, J., Thieme, J., Neuhäusler, U., Susini, J. & Kögel-Knabner, I. (2003). *Eur. J. Soil Sci.* **54**, 423–433.
- Prietzl, J., Tyufekchieva, N., Eusterhues, K., Kögel-Knabner, I., Thieme, J., Paterson, D., McNulty, I., de Jonge, M., Eichert, D. & Salomé, M. (2009). *Geoderma*, **153**, 318–330.
- Ravel, B. & Newville, M. (2005). *J. Synchrotron Rad.* **12**, 537–541.
- Starkey, R. L. (1965). *Soil Sci.* **101**, 297–306.
- Turner, L. J. & Kramer, J. R. (1992). *Water Air Soil Poll.* **63**, 23–32.